J Fluoresc (2010) 20:745–751
DOI 10.1007/s10895-010-0617-1

ORIGINAL PAPER

Spectroscopic Properties and Energy Transfer Analysis of Tm^{3+}-Doped BaF_2-Ga_2O_3-GeO_2-La_2O_3 Glass

Shenglei Yu · Zhongmin Yang · Shanhui Xu

Received: 19 May 2009 / Accepted: 7 February 2010 / Published online: 4 March 2010

Abstract This paper reports on the spectroscopic properties and energy transfer analysis of Tm^{3+}-doped BaF_2-Ga_2O_3-GeO_2-La_2O_3 glasses with different Tm_2O_3 doping concentrations (0.2, 0.5, 2.0, 2.5, 3.0, 3.5, 3.5, 4.0 wt%). Mid-IR fluorescence intensities in the range of 1,300 nm −2,200 nm have been measured when excited under an 808 nm LD for all the samples with the same pump power. Energy level structure and Judd-Ofelt parameters have been calculated based on the absorption spectra of Tm^{3+}, cross-relaxation rates and multi-phonon relaxation rates have been estimated with different Tm_2O_3 doping concentrations. The maximum fluorescence intensity at around 1.8 μm has been obtained in Tm_2O_3-3 wt% sample and the maximum value of calculated stimulated emission cross-section of Tm^{3+} in this sample is about 0.48×10^{-20} cm^2 at 1,793 nm, and there is not any crystallization peak in the DSC curve of this sample, which indicate the potential utility of Tm^{3+}-doped BaF_2-Ga_2O_3-GeO_2- La_2O_3 glass for 2.0-μm optical fiber laser.

Keywords Tm^{3+}-doped BaF_2-Ga_2O_3-GeO_2-La_2O_3 glass · Spectroscopic properties · Energy transfer process · Judd-Ofelt theory · Stimulated emission cross-section

Introduction

2.0-μm laser has many potential applications in remote sensing, laser radar, surgery in medicine, material processing, ultra-low-loss-long-span communication [1–6]. As the transition of $^3F_4 \rightarrow {}^3H_6$ of trivalent thulium can generate radiations near 2.0-μm, in recent few years, Tm^{3+}-doped laser materials have been widely studied. At least three reasons can be accounted for it [7]: (1) the strong absorption band of Tm^{3+} around 800 nm overlaps with the fluorescence band of high power commercially available AlGaAs laser diodes; (2) with high doping concentration, the theoretical quantum efficiency of Tm^{3+}-doped optical fiber laser is nearly 200% due to the strong cross- relaxation ($^3H_6$, $^3H_4 \rightarrow {}^3F_4$, $^3F_4$); (3) the lasing range of Tm^{3+}-doped fiber lasers can be tuned over a wide range.

To get efficient Tm^{3+}-doped 2.0-μm optical fiber laser, some factors should be considered for the glass host, such as the highest phonon energy, environmental durability, fiber drawing ability, rare-earth ion solubility and the purity of the starting materials [8, 9]. Many glass hosts have been successfully used for Tm^{3+}-doped 2-μm optical fiber laser, such as silica glasses [2, 3, 8, 10], fluoride glasses [11–14]. Though silica glasses have excellent mechanical strength and environmental durability, the low rare-earth durability (less than 1,000 ppm), especially the large highest phonon energy (~1,100 cm^{-1}) [15] limit the laser efficiency. The small phonon energy (~500 cm^{-1}) [15] make fluoride glasses attractive as the glass hosts for Tm^{3+}-doped 2.0-μm optical fiber laser, but its poor mechanical strength, bad environmental durability and low laser damage threshold limit its application.

Heavy metal oxide glasses have good mechanical strengths, high rare-earth ions solubility and moderate highest phonon energy. Of these, Barium Gallo-Germanate (BGG) glass is one type of glasses with good glass forming ability and thus BGG glass would be a good host material for Tm^{3+}-doped 2.0-μm optical fiber laser. But until now few reports have focused on Barium Gallo-Germanate (BGG) to seek for the possibility of its potential application in 2.0-μm

S. Yu · Z. Yang (✉) · S. Xu
Institute of Optical Communication Materials, Key Laboratory of Special Functional Materials of Ministry of Education, South China University of Technology, Guangzhou 510641, People's Republic of China
e-mail: yangzm@scut.edu.cn
e-mail: yslei168@yahoo.com.cn

optical fiber laser. In the present paper, we have focused on the spectroscopic properties and energy transfer analysis of Tm^{3+}-doped BGG glasses due to its good mechanical strength and environmental durability, moderate highest phone energy (~900 cm^{-1}).

Experimental

The glass composition is 15BaO-11Ga_2O_3-70GeO_2-4La_2O_3 (mol %) (BGGL), Tm_2O_3 was added externally with different concentrations (0.2, 0.5, 2.0, 2.5, 3.0, 3.5, 4.0 wt%). In Tm^{3+}- doped laser materials, a low OH^- content is important to reduce the non-radiative energy transfer from the excited state of Tm^{3+} ion to OH^- radicals [16] and thus BaF_2 was used to totally replace BaO in the raw materials to reduce the OH^- content. The raw materials include reagent grade BaF_2 (>99%), high purity Ga_2O_3 (>99.99%), GeO_2 (>99.999%), La_2O_3 (>99.99%) and Tm_2O_3 (>99.99%). Batches of 15 g mixture powders have been melted in quartz crucibles with covers at 1,450 °C for 40 min in a SiC-heater furnace within ambient atmosphere. All the melted glass samples were kept heating at 600 °C for at least 2 h, and then annealed to room temperature gradually; finally they were cut and polished into the size of 20 mm×10 mm×1.5 mm for optical measurements and 20 mm×10 mm×0.7 mm for the lifetime measurements of the $^3H_4$ state.

Absorption spectra of the Tm^{3+}-doped BGGL glasses were measured by Perkin-Elmer Lambda 900 UV-Vis-NIR spectral photometer in the range of 300–3,300 nm. Infrared fluorescence spectra of the bulk glass samples were measured by a Triax 320 spectro- fluorimeter (Jobin-Yvon Corp.) under the excitation of an 808 nm LD (Coherent Corp.) with the output power of 1 W, the signals were collected by a PbSe detector at room temperature, using a standard SR510 lock-in amplifier. Lifetimes of the $^3H_4$ state were obtained from the decay curves of the $^3H_4 \rightarrow {}^3F_4$

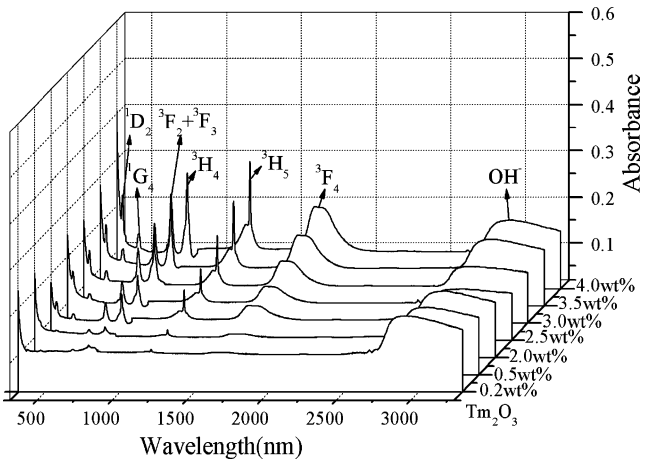

Fig. 1 Absorption spectra of Tm^{3+}-doped BGGL glasses

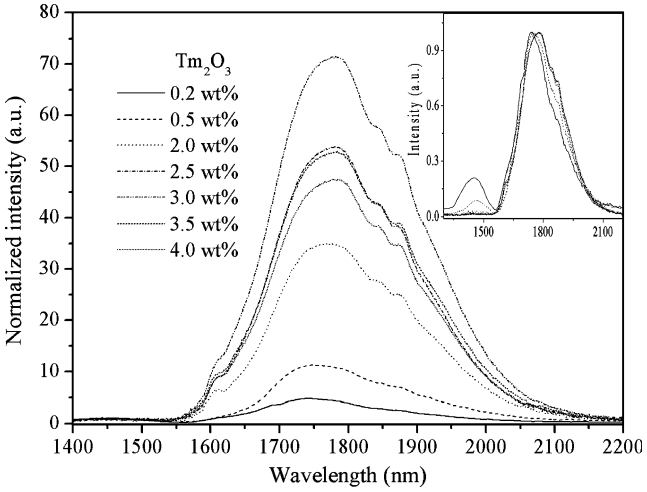

Fig. 2 Normalized fluorescence spectra of Tm^{3+}-doped BGGL glasses

fluorescence at 1.46 μm by using a computer controlled digitizing oscilloscope and an InGaAs detector. Refractive index of the samples was recorded on a prism coupling apparatus (Metricon 2010). Thermal property of the glass were determined by using a Netzsch STA 449C Jupiter differential scanning calorimeter (DSC) at a heating rate of 10 K/min from temperature to 900 °C.

Results and discussions

Spectroscopic properties of Tm^{3+}-doped BGGL glasses

Figure 1 shows the absorption spectra of Tm^{3+}-doped BGGL glass samples with different Tm_2O_3 doping concentrations (0.2, 0.5, 2.0, 2.5, 3.0, 3.5, 4.0wt%). Six well-resolved peaks at around 1,670 nm, 1,210 nm, 790 nm, 660 nm and 682 nm, 468 nm, 356 nm can be observed, corresponding to the ground state absorption of the state $^3F_4$, $^3H_5$, $^3H_4$, $^3F_2$ and $^3F_3$, $^1G_4$, $^1D_2$ respectively. Additionally, there is a wide OH^- absorption peak at around 2.9 μm.

Figure 2 shows the fluorescence spectra of Tm^{3+}-doped BGGL glass samples. Obviously, the fluorescence intensities at around 1.46 μm due to the $^3H_4 \rightarrow {}^3F_4$ transitions are very weak, and the maximum intensity at around 1.8 μm due to the $^3F_4 \rightarrow {}^3H_6$ transition has been obtained in the Tm_2O_3-3 wt% sample.

Judd-Ofelt analysis of Tm^{3+}-doped BGGL glasses

Three Judd-Ofelt intensity parameters Ω_λ (λ=2,4,6) have been obtained from the line strengths of electronic dipole (S_{ed}) transition using a least-squares fitting [17]:

$$S_{ed}(J:J') = \sum_{\lambda=2,4,6} \Omega_\lambda \left| < f^n[\alpha SL]J \left\| U^{(\lambda)} \right\| f^n[\alpha' S'L']J' > \right|^2 \quad (1)$$

Where J and J' are the total angular momentum of the initial and terminal states, αSL define all other quantum numbers needed to specify the states. $U^{(\lambda)}$ are the reduced matrix elements. The fitting quality can be estimated by the root-mean-square deviation δ_{rms} [18]:

$$\delta_{rms} = \left[\frac{\sum (\Delta f)^2}{n_{transitons} - n_{parameters}}\right]^{1/2} \quad (2)$$

The line strength for a magnetic dipole (MD) transition can be calculated as [17]:

$$S_{md}(J,J') = \left(\frac{h}{2\pi m_e c}\right)^2 |< f^n[\alpha SL]J\|\mathrm{L} + 2\mathrm{S}\|f^n[\alpha' S'L']J' >|^2 \quad (3)$$

Where h is the Planck constant, m_e is the mass of the electron, c is the velocity of the light. The matrix elements for MD transition are impossible, if and only if $\Delta S = \Delta L$, $\Delta J = 0$ or ± 1.

Using the calculated S_{ed} and S_{md}, spontaneous transition probabilities A (aJ: bJ'), fluorescence branching ratio β (aJ: bJ') and radiative lifetime τ_r from the initial to the terminal state can be calculated as [17]:

$$A(aJ:bJ') = \frac{64\pi^4 e^2}{3h(2J+1)\lambda^3}\left[\frac{n(n^2+2)^2}{9}S_{ed}(aJ:bJ') + n^3 S_{md}(aJ:bJ')\right] \quad (4)$$

$$\beta[aJ:bJ'] = \frac{A(aJ:bJ')}{\sum_{bJ'} A(aJ:bJ')} \quad (5)$$

$$\tau_r = \left\{\sum_{S'L'J'} A[(S,L)J:(S',L')J')]\right\}^{-1} = A_{total}^{-1} \quad (6)$$

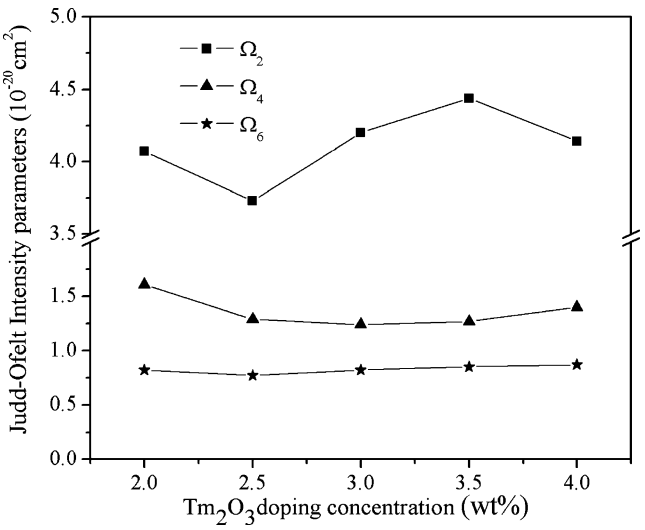

Fig. 3 Judd-Ofelt intensity parameters of Tm^{3+}-doped BGGL glasses

Table 1 Comparison of Judd-Ofelt parameters of Tm^{3+}-doped glass hosts

Glass host	Ω_2 ($\times 10^{-20}$cm^2)	Ω_4 ($\times 10^{-20}$cm^2)	Ω_6 ($\times 10^{-20}$cm^2)	References
Fluoride	2.02	1.56	1.10	[19]
Phosphate	5.88	2.88	1.14	[19]
Borate	5.42	2.78	1.66	[19]
Tellurite	4.69	1.83	1.14	[20]
GBPG	2.84	0.50	0.75	[20]
BGGL (Tm_2O_3-3 wt%)	4.11	1.21	0.80	This work

Where e is the charge of the electron, n is the refractive index, λ is the mean wavelength of the absorption band. As the small absorption bands would lead to large deviations to Judd-Ofelt parameters, Judd-Ofelt analysis were only used for samples with Tm_2O_3 doping concentration higher than 0.5 wt%, the reduced matrix elements derived in Ref. [18]. As can be seen from Fig. 1, $^3F_2$ and $^3F_3$ states are difficult to be resolved individually; they have been treated as a single state, the sum value of their matrix elements have been used for calculation. Judd-Ofelt parameters have been obtained from five absorption bands ($^1D_2$, $^1G_4$, $^3F_2$ and $^3F_3$, $^3H_4$, $^3F_4$). Figure 3 shows the calculated Judd-Ofelt parameters of Tm^{3+}-doped BGGL glasses with different Tm_2O_3 doping concentrations (2.0, 2.5, 3.0, 3.5, 4.0 wt%). The values of Ω_2 are in the range of 3.54–4.26$\times 10^{-20}$ cm^2, values of Ω_4 and Ω_6 varied slightly with the increase of Tm_2O_3 doping concentration. The mean squared deviations are 0.04×10^{-6}, 0.03×10^{-6}, 0.28×10^{-6}, 0.35×10^{-6}, and 0.18×10^{-6} respectively.

Judd-Ofelt parameters of Tm^{3+}-doped different glass hosts have been summarized in Table 1. Obviously, the Ω_2 values of Tm^{3+}-doped BGGL glass are larger than values of Ga_2O_3- $B_{i2}O_3$-PbO-GeO_2 and fluoride glass, but smaller than values of other oxide (phosphate, borate and tellurite) glasses. As Ω_2 value is an indicative of the amount of covalent bonding, and Ω_6 value is related to the rigidity of the host [19], the value of Ω_6 in this work indicate that the rigidity of the glass host don't changes much after the introduction of Tm_2O_3. Table 2 shows the Energy gap (ΔE), line strength of electronic dipole (S_{ed}), transition probability ($A_{JJ'}$), branching ratio ($\beta_{JJ'}$) and radiative lifetimes (τ_r) of Tm^{3+} in the Tm_2O_3-3 wt% sample.

Energy transfer among Tm^{3+} in BGGL glasses

For the weak fluorescence intensities at around 1.46 μm, three possible non- radiative decay processes can be contributed for it: cross-relaxation ($^3H_4$, $^3H_6 \rightarrow {}^3F_4$, $^3F_4$) and multi-phonon relaxation [9, 21], as well as resonant energy transfer [22].

Table 2 Calculated energy gap (ΔE), line strength (S_{ed}), transition probability ($A_{JJ'}$), branching ratio ($\beta_{JJ'}$) and radiative lifetimes (τ_r) of BGGL glass with 3 wt% Tm_2O_3

Transitions	Energy gap ΔE (cm^{-1})	Line strength S_{ed}($\times 10^{-20} cm^2$)	Transition probability $A_{JJ'}$(s^{-1})	Branching ratio $\beta_{JJ'}$	Radiative lifetimes τ_r (μs)
$^3F_4 \rightarrow {}^3H_6$	5952.4	3.9034	303.5066	1	4,104
$^3H_5 \rightarrow {}^3H_6$	8264.5	1.3242	329.912	0.978	
$^3H_5 \rightarrow {}^3F_4$	2312.1	1.3254	7.2656	0.022	4,044
$^3H_4 \rightarrow {}^3H_6$	12658.2	1.8229	1744.8451	0.921	
$^3H_4 \rightarrow {}^3F_4$	6705.8	0.993	125.8863	0.066	818
$^3H_4 \rightarrow {}^3H_5$	4393.7	0.6693	23.4589	0.012	
$^3F_3 \rightarrow {}^3H_6$	14639.1	1.0211	2045.4774	0.752	
$^3F_3 \rightarrow {}^3F_4$	8686.7	0.1374	189.8005	0.07	
$^3F_3 \rightarrow {}^3H_5$	6374.6	3.7352	482.5576	0.19	
$^3F_3 \rightarrow {}^3H_4$	1980.9	1.0897	3.9993	0.001	496
$^3F_2 \rightarrow {}^3H_6$	15174.5	0.1909	865.4978	0.415	
$^3F_2 \rightarrow {}^3F_4$	9222.1	1.6791	981.3078	0.471	
$^3F_2 \rightarrow {}^3H_5$	6,910	0.7963	215.6277	0.103	
$^3F_2 \rightarrow {}^3H_4$	2516.3	1.942	23.1333	0.011	
$^3F_2 \rightarrow {}^3F_3$	535.4	0.2969	0.0273	0	762
$^1G_4 \rightarrow {}^3H_6$	21390.4	0.3561	1235.2992	0.396	
$^1G_4 \rightarrow {}^3F_4$	15,438	0.2618	438.7408	0.141	
$^1G_4 \rightarrow {}^3H_5$	13125.9	0.7854	1011.6692	0.324	
$^1G_4 \rightarrow {}^3H_4$	8732.2	1.1004	361.7969	0.116	
$^1G_4 \rightarrow {}^3F_3$	6751.3	0.3633	59.8289	0.019	
$^1G_4 \rightarrow {}^3F_2$	6215.9	0.153	11.5674	0.004	458
$^1D_2 \rightarrow {}^3H_6$	28248.6	0.46	4190.218	0.69	
$^1D_2 \rightarrow {}^3F_4$	22296.2	3.3109	28098.977	0.833	
$^1D_2 \rightarrow {}^3H_5$	19984.1	0.0142	129.0559	0.004	
$^1D_2 \rightarrow {}^3H_4$	15590.4	0.8532	2763.9267	0.078	
$^1D_2 \rightarrow {}^3F_3$	13609.5	0.955	1707.0568	0.046	
$^1D_2 \rightarrow {}^3F_2$	13074.1	0.7209	782.3016	0.021	
$^1D_2 \rightarrow {}^1G_4$	6858.2	1.182	253.9052	0.008	34

Figure 4 shows the energy level structure and cross-relaxation process of Tm^{3+} in BGGL glasses. Figure 5 shows the normalized fluorescence ($^3H_4 \rightarrow {}^3F_4$) and absorption ($^3H_6 \rightarrow {}^3F_4$) spectra of the Tm_2O_3-0.5 wt% sample. As can be seen from Fig. 5, there is a small spectral overlap between the fluorescence and absorption spectra, which indicates resonant energy transfer would occur among Tm^{3+}. Han and co-workers [22] studied the energy transfer process due to the small spectra overlap in Tm^{3+}-doped germanate glasses under different temperature, they concluded that the contribution of energy transfer due to the small spectral overlap is minimal.

The calculated energy mismatch between the two transitions ($^3H_4 \rightarrow {}^3F_4$ and $^3H_6 \rightarrow {}^3F_4$) is about 930 cm^{-1}, which indicates cross-relaxation process requires the assistance of phonons [9]. Figure 2 also shows that the fluorescence intensity at around 1.46 μm in the Tm_2O_3-0.2 wt% sample is much higher than those in other samples; therefore cross-relaxation in the Tm_2O_3- 0.2 wt% sample can be neglected compared with other samples.

Figure 6 shows the measured fluorescence lifetimes of the $^3H_4$ state of Tm^{3+} in BGGL glasses. Obviously, with the increase of Tm_2O_3 doping concentration, measured fluorescence lifetimes decreased. If the resonant energy transfer process can be neglected, using the measured fluorescence lifetimes of $^3H_4$ states and radiative lifetimes calculated by Judd-Ofelt theory, cross-relaxation and multi-phonon relaxation rates can be estimated as follows [22]:

$$W_{CR} = \frac{1}{\tau_m(xwt\%)} - \frac{1}{\tau_m(0.2wt\%)} \tag{7}$$

$$W_{MPR} = \frac{1}{\tau_m} - \frac{1}{\tau_r} - W_{CR} \tag{8}$$

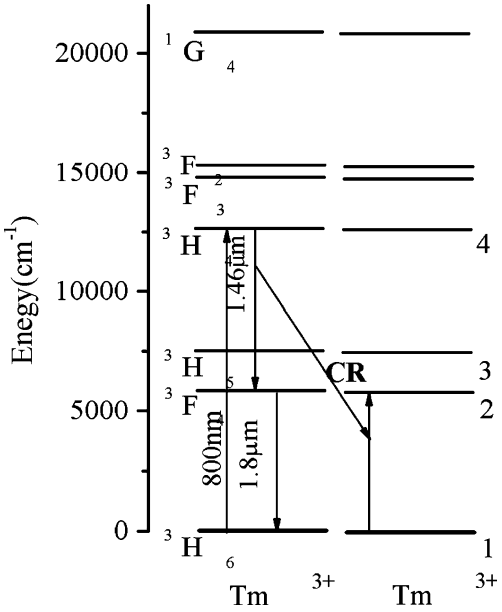

Fig. 4 The energy level structure and cross-relaxation process of Tm^{3+} in BGGL glass

Where W_{CR} is the cross-relaxation rate, τ_m is the measured lifetime of the $^3H_4$ states, x is the doping concentration of Tm_2O_3 higher than 0.2, W_{MPR} is the multi- phonon relaxation rate, and τ_r is the calculated lifetime of $^3H_4$ states using Judd-Ofelt theory. Table 3 shows the measured and calculated results of Tm^{3+} in BGGL glasses.

As can be seen from Table 3, for the $^3H_4 \rightarrow {}^3F_4$ transitions, with the increase of Tm_2O_3 doping concentration, cross-relaxation rates increase rapidly, but multi-phonon relaxation rates are considered to be unchanged within the calculation error and they are much lower than cross-relaxation rates, especially in samples with Tm_2O_3 doping concentrations higher than 2.5 wt%.

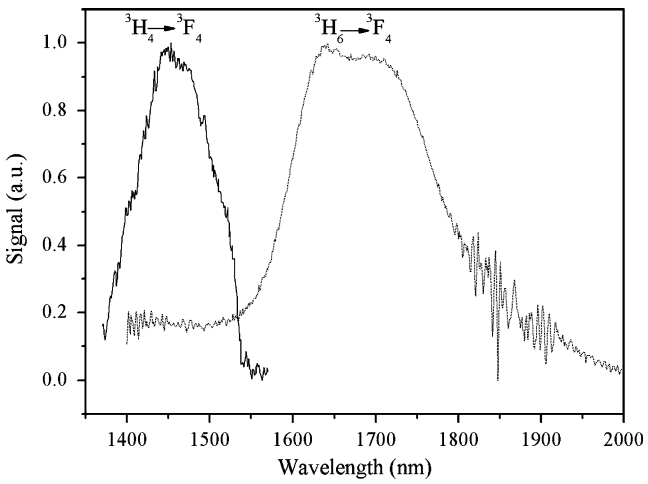

Fig. 5 The normalized fluorescence and absorption spectra of Tm^{3+} in BGGL glass (Tm_2O_3-0.5 wt%)

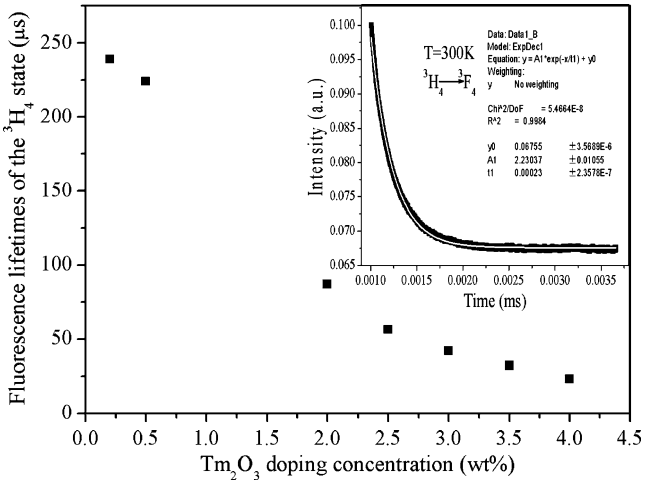

Fig. 6 The measured fluorescence lifetimes of the $^3H_4$ state of Tm^{3+} in BGGL glasses

For the $^3F_4 \rightarrow {}^3H_6$ transitions, results in Table 3 show that fluorescence integration intensity value of the Tm_2O_3-3 wt% sample is about 7.75 times of the value obtained in the Tm_2O_3- 0.2 wt% sample. If multi-phonon relaxation rates between $^3F_4$ and $^3H_6$ states can be neglected compared with cross-relaxation rates, the maximum fluorescence intensity obtained in Tm_2O_3-3 wt% sample indicate the highest fluorescence quantum efficiency of this sample among all of the Tm^{3+}-doped BGGL glasses.

Absorption and stimulated emission cross-section of Tm^{3+}-doped BGGL glass

Absorption cross-section (σ_a) was determined from the absorption spectra using Beer-Lambert equation [23]:

$$\sigma_a(\lambda) = \frac{1}{Nl} \ln\left(\frac{I_0}{I}\right) \tag{9}$$

Where N is Tm^{3+}doping concentration, l is the thickness of the sample, I_0 and I are the intensities of the incident and transmitted light respectively. Stimulated emission cross-section (σ_e) was calculated from the fluorescence spectrum by using the Fuchtbauer- Ladenburg (F-L) formula [23]:

$$\sigma_e^{FL}(\lambda) = \frac{\lambda^5}{8\pi c n^2} A_r g(\lambda) \tag{10}$$

Where β is the branching ratio (for the $^3F_4$ level, β=1), A_r is the radiative transition probability, and $g(\lambda)$ is the normalized line-shape function obtained from the measured fluorescence spectrum [23].

Figure 7 shows the absorption and stimulated emission cross-section of Tm^{3+} for the $^3F_4 \rightarrow {}^3H_6$ transition in BGGL glasses with 3 wt% Tm_2O_3, the peak emission cross-section occurs around 1,793 nm, with a value of 0.48×10^{-20} cm^2, larger than values in other glass systems: 0.41×10^{-20} cm^2 in

Table 3 Measured and calculated results of Tm^{3+} in BGGL glasses

Sample	x (wt%)	$^3H_4$ τ_m (μs)	$^3H_4$ τ_r (μs)	W_{CR} (s^{-1})	W_{MPR} between $^3H_4$ and $^3F_4$ states (s^{-1})	$^3F_4$ τ_r (μs)	Fluorescence integration intensity of $^3F_4 \rightarrow {}^3H_6$ transition (1,530–2,200nm)
BGGL02	0.2	239	–	–	–	–	349.0
BGGL05	0.5	224	–	280.2	–	–	553.9
BGGL20	2.0	87	822	7310.2	2967.6	3,926	1517.7
BGGL25	2.5	56	900	13673.0	3073.0	4,439	2016.2
BGGL30	3.0	42	818	19625.4	2961.6	4,104	2703.8
BGGL35	3.5	32	777	27065.9	2897.1	3,901	2221.5
BGGL40	4.0	23	795	39294.2	2926.2	3,956	2009.6

GGBP glass [20], 0.37×10^{-20} cm^2 in oxyfluoride precursor glass [23], 0.32×10^{-20} cm^2 in tellurite glass [24], 0.42×10^{-20} cm^2 in lead germanate glass [25].

Thermal property of Tm^{3+}-doped BGGL glass

Figure 8 shows the DSC curve of Tm^{3+}-doped BGGL glass with Tm_2O_3 doping concentration of 3 wt%. The glass transition temperature (T_g) is about 672 °C, and there is no evident crystallization peak on the DSC curve, which indicate the good fiber drawing ability of this glass.

Conclusions

In summary, we have investigated the spectroscopic properties and energy transfer processes of Tm^{3+}-doped BGGL glasses with different Tm_2O_3 doping concentrations (0.2, 0.5, 2.0, 2.5, 3.0, 3.5, 4.0 wt%) at room temperature. Due to the strong cross- relaxation, for samples with Tm_2O_3 doping concentration higher than 0.5 wt%, fluorescence intensities at around 1.46 μm are very weak, and the maximum fluorescence intensity at around 1.8 μm was obtained in the Tm_2O_3-3.0 wt% sample. Energy transfer analysis show that, with the increase of Tm_2O_3 doping concentration, cross-relaxation rates would increase rapidly, but multi-phonon relaxation rates changed slightly and they are much lower than cross-relaxation rates, the highest fluorescence quantum efficiency also obtained in the Tm_2O_3-3.0 wt% sample. The stimulated emission cross-section exhibit a maximum value of 0.48×10^{-20} cm^2 at around 1,793 nm, and thermal property result shows there is not evident crystallization peak on the DSC curve of the Tm_2O_3-3 wt% sample, which indicate the potential of Tm^{3+}-doped BGGL glass for 2.0 μm optical fiber laser.

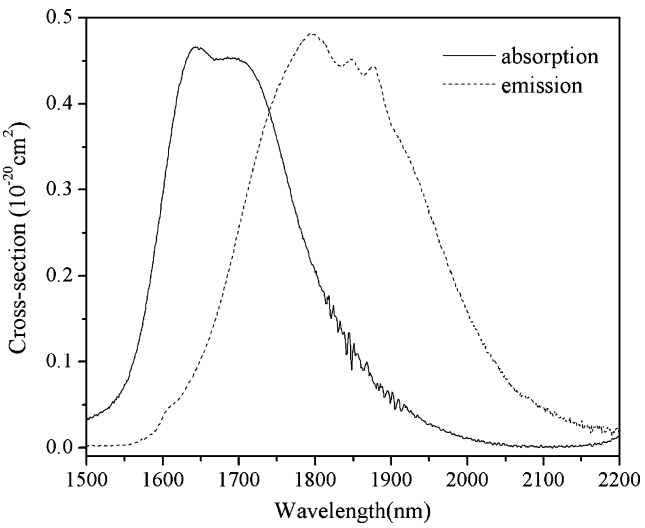

Fig. 7 Absorption and stimulated emission cross-section of Tm^{3+} in BGGL glass (Tm_2O_3-3 wt%)

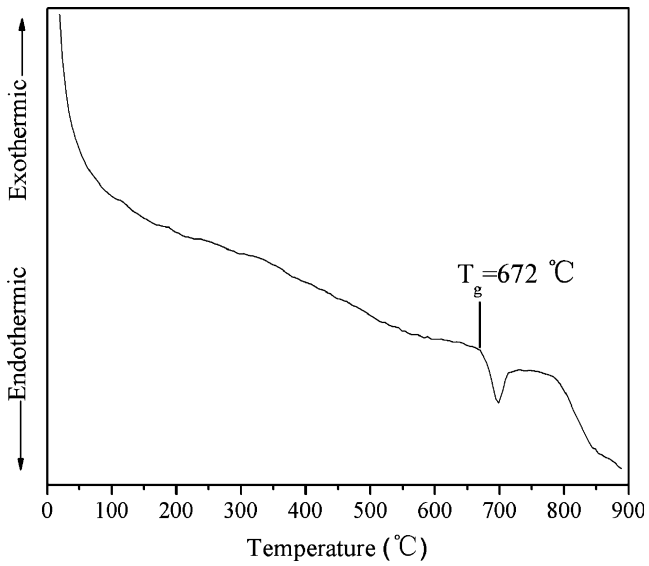

Fig. 8 DSC curve of Tm^{3+}-doped BGGL glass (Tm_2O_3-3 wt%)

Acknowledgement This work is supported by the DSTG (2006Z2-D0161), DSTG (2006 J1-C0491) and NSFC (50602017).

References

1. Henderson SW, Suni PJM, Hale CP, Hannon SM, Magee JR, Bruns DL, Yuen EH (1993) Coherent laser radar at 2-μm using solid-state lasers. IEEE Trans Geosci Remote Sens 31:4–15. doi:10.1109/36.210439
2. Shen DY, Sahu JK, Clarkson WA (2006) High-power widely tunable Tm: fiber lasers pumped by an Er, Yb co-doped fiber laser at 1.6 μm. Opt Express 14:6084–6090. doi:10.1364/OE.14.006084
3. Wu JF, Jiang SB, Luo T, Geng JH, Peyghambarian N, Barnes NP (2006) Efficient thulium-doped 2 μm germanate fiber laser. IEEE Photonic Technol Lett 18:334–336. doi:10.1109/LPT.2005.861970
4. Xavier M, Valentin P, Liu JH, Maria C, Uwe G, Magdalena A, Francesc D, Miguel G, Gregorio V (2006) Efficient 2-μm continuous-wave laser oscillation of Tm^{3+}:$Klu(WO_4)_2$. IEEE Quant Electron 42:1008–1015. doi:10.1109/JQE.2006.881629
5. Hayward RA, Clarkson WA, Turner PW, Nilsson J, Grudinin AB, Hanna DC (2000) Efficient cladding-pumped Tm doped silica fibre laser with high power singlemode output at 2 μm. Electron Lett 32:711–712. doi:10.1049/el:20000577
6. Geng JH, Wu JF, Jiang SB, Yu JR (2007) Efficient operation of diode-pumped single-frequency thulium-doped fiber lasers near 2 μm. Opt Lett 32:355–357. doi:10.1364/OL.32.000355
7. Liu G (USA) Jacquier B (France) (2005) Spectroscopic Properties of Rare Earths in Optical Materials. Tsinghua University Press. ISBN 7-302-07409-7: 364–365
8. Tsang YH, Coleman DJ, King TA (2003) High power 1.9 μm Tm^{3+}-silica fibre laser pumped at 1.06 μm by a Yb^{3+}-silica fibre laser. Opt Commun 231:357–364. doi:10.1016/j.optcom.2003.11.072
9. Balda R, Fernandez J, Arriandiaga MA, Lacha LM, Fernandez-Navarro JM (2006) Effecet of concentration on the infrared emissions of Tm^{3+} ions in lead niobium germanate glasses. Opt Mater 28:1253–1257. doi:10.1016/j.optmat.2005.11.033
10. Jackson SD (2004) Cross relaxation and energy transfer upconversion processes relevant to the functioning of 2 μm Tm^{3+}-doped silica fibre lasers. Opt Commun 230:197–203. doi:10.1016/j.optcom.2003.11.045
11. Carter JN, Snart RG, Hanna DC, Tropper AC (1990) CW diode-pumped operation of 1.97 μm thulium-doped fluorozirconate fiber laser. Electron Lett 26:599–601. doi:10.1049/el:19900394
12. Percival RM, Szebestaand D, Davey ST (1992) Highly efficient and tunable operation of two colour Tm-doped fluoride fiber laser. Electron Lett 28:671–673. doi:10.1049/el:19920424
13. Yamamoto T, Miyajima Y, Komukai T, Sugawa T (1993) 1.9 μm Tm-doped fluoride fibre amplifier and laser pumped at 1.58 μm. Electron Lett 29:986–987. doi:10.1049/el:19930656
14. Percival RM, Szebesta D, Seltzer CP, Perrin SD, Davey ST, Louka M (1995) A 1.6-μm pumped 1.9-μm thulium-doped fluoride fiber laser and amplifier of very high efficiency. IEEE J Quantum Electron 31:489–493. doi:10.1109/3.364404
15. Pollnau M, Jackson SD (2003) Solid-state mid-infrared laser sources. Springer- Verlag Berlin Heidelberg. ISBN 978-3-540-00621-3. 89:219–255
16. Jackson SD, Mossman S (2003) Efficiency dependence on the Tm^{3+} and Al^{3+} concentrations for Tm^{3+}-doped silica double-clad fiber lasers. Appl Opt 42:2702–2707. doi:10.1364/AO.42.002702
17. Walsh BM, Barnes NP, Bartolo BD (1998) Branching ratios, cross sections, and radiative lifetimes of rare earth ions in solids: application to Tm^{3+} and Ho^{3+} ions in $LiYF_4$. J Appl Phys 83:2772–2787. doi:10.1063/1.367037
18. Tanabe S, Tamai K, Hirao K, Soga N (1993) Excited-state absorption mechanisms in red-laser-pumped uv and blue upconversions in Tm^{3+}-doped fluoroaluminate glass. Phys Rev B 47:2507–2514. doi:10.1103/PhysRevB.47.2507
19. Yeh DC, Petrin RR, Sibley WA, Madigou V, Adam JL, Suscavage MJ (1989) Energy transfer between Er^{3+} and Tm^{3+} ions in a barium fluoride-thorium fluoride glass. Phys Rev B 39:80–90. doi:10.1103/PhysRevB.39.80
20. Shi DM, Zhang QY, Yang GF, Jiang ZH (2007) Spectroscopic properties and energy transfer in Ga_2O_3-Bi_2O_3-PbO-GeO_2 glasses codoped with Tm^{3+} and Ho^{3+}. J Non-Cryst Solids 353:1508–1514. doi:10.1016/j.jnoncrysol.2007.02.034
21. Balda R, Fernández J, García-Revilla S, Fernández-Navarro JM (2007) Spectroscopy and concentration quenching of the infrared emissions in Tm^{3+}-doped TeO_2-TiO_2- Nb_2O_5 glass. Opt Express 15:6750–6761. doi:10.1364/OE.15.006750
22. Han YS, Song JH, Heo J (2003) Analysis of cross relaxation between Tm^{3+} ions in PbO-Bi_2O_3-Ga_2O_3-GeO_2 glass. J Appl Phys 94:2817–2820. doi:10.1063/1.1595148
23. Shin YB, Lim HT, Choi YG, Kim YS, Heo J (2000) 2.0 μm Emission properties and energy transfer between Ho^{3+} and Tm^{3+} in PbO-Bi_2O_3-Ga_2O_3 glasses. J Am Ceram Soc 83:787–791
24. Yamauchi H, Murugan GS, Ohishi Y (2005) Optical properties of Er^{3+} and Tm^{3+} ions in a tellurite glass. J Appl Phys 97:043505-043505-8
25. Shepherd DP, Brinck DJB, Wang J, Tropper AC, Hanna DC, Kakarantzas G, Townsend PD (1994) 1.9-μm operation of a Tm: lead germanate glass waveguide laser. Opt Lett 19:954–956. doi:10.1364/OL.19.000954